



Glass fracture by focusing of laser-generated nanosecond surface acoustic waves

David Veyssset^{a,b,*}, Steven E. Kooi^a, Ryadh Haferssas^{a,c}, Mostafa Hassani-Gangaraj^d, Mohammad Islam^{a,c}, A.A. Maznev^{a,b}, Yevheniia Chernukha^e, Xiaoguang Zhao^f, Keiichi Nakagawa^{g,i}, Dmitro Martynowych^{a,b}, Xin Zhang^f, Alexey M. Lomonosov^h, Christopher A. Schuh^d, Raul Radovitzky^{a,c}, Thomas Pezeril^d, Keith A. Nelson^{a,b}

^a Institute for Soldier Nanotechnologies, Massachusetts Institute of Technology, Cambridge, MA 02139, USA

^b Department of Chemistry, Massachusetts Institute of Technology, Cambridge, MA 02139, USA

^c Department of Aeronautics and Astronautics, Massachusetts Institute of Technology, Cambridge, MA 02139, USA

^d Department of Materials Science and Engineering, Massachusetts Institute of Technology, Cambridge, MA 02139, USA

^e Institut Molécules et Matériaux du Mans, UMR CNRS 6283, Université du Maine, 72085 Le Mans, France

^f Department of Mechanical Engineering, Boston University, Boston, MA 02215, USA

^g Department of Bioengineering, The University of Tokyo, Tokyo 113-8656, Japan

^h Prokhorov General Physics Institute RAS, Moscow, Russia

ⁱ Department of Precision Engineering, The University of Tokyo, Tokyo 113-8656, Japan

ARTICLE INFO

Article history:

Received 10 July 2018

Accepted 14 August 2018

Available online 29 August 2018

Keywords:

Dynamic fracture
Surface acoustic waves
Interferometry
Glass

ABSTRACT

Dynamic fracture of borosilicate glass through focusing of high-amplitude nanosecond surface acoustic waves (SAWs) at the micron scale is investigated in an all-optical experiment. SAWs are generated by a picosecond laser excitation pulse focused into a ring-shaped spot on the sample surface. Interferometric images capture the SAW as it converges towards the center, focuses, and subsequently diverges. Above a laser energy threshold, damage at the acoustic focal point is observed. Numerical calculations help us determine the time evolution of the stress distribution. We find that the glass withstands a local tensile stress of at least 6 GPa without fracture.

© 2018 Acta Materialia Inc. Published by Elsevier Ltd. All rights reserved.

The dynamic fracture of glassy materials is of great importance for a wide range of technologic applications, from cracked mobile device screens or car windshields hit by rocks on the road to the International Space Station's windows subjected to space debris impacts [1]. Glasses, despite being intrinsically among the strongest man-made materials, are vulnerable through their defects, which can reduce the static tensile strength by orders of magnitude [2]. While the theoretical tensile strength limit of silica glass is about 20 GPa [3], experimentally-measured static tensile strength can be as low as 0.1–0.2 GPa in bulk specimens [4]; in nanoscale specimens that sample few or no flaws much higher tensile strengths exceeding 10 GPa can be measured [5]. When dealing with high strain rate situations (e.g. an impact of a micro-meteorite on a spacecraft), static material properties offer only limited insight into materials resistance to crack initiation and propagation [6]. Dynamic fracture of silicate glasses on the microsecond time scale has been extensively studied in shock spallation experiments under

plate [7–10] or laser-induced shock [11]. These measurements, in which spallation is caused by tensile stresses in release waves, reveal a much higher tensile strength under dynamic loading, typically in the few GPa range. For example, the reported spall strength of soda lime glass ranges from 2.2 to over 5 GPa [7,9,11]. The interpretation of tensile strength measurements in plate impact experiments is complicated by the fact that the material is initially subjected to compression; above ~4 GPa many studies report an apparent structural degradation under compression (“failure waves”) [8–10,12–14], which reduces the subsequently measured tensile strength on release. It is evident that the dynamic strength of glass is not a material constant; rather, it depends on the duration of the tensile stress and on the entire loading history. Whereas laser shock experiments on metals such as aluminum and copper [15] indicate that under very short (sub-nanosecond) shock pulses, the spall strength approaches the theoretical limit for those materials, it remains an open and practically relevant question whether the theoretical limit can be approached for silicate glasses.

In this work, we describe a methodology for studying glass failure on the nanosecond time scale using focusing laser-generated surface acoustic waves (SAWs). High amplitude SAWs have already been

* Corresponding author at: Institute for Soldier Nanotechnologies, Massachusetts Institute of Technology, Cambridge, MA 02139, USA.
E-mail address: dveysset@mit.edu (D. Veyssset).

proven capable of causing fracture in brittle materials [16,17]. In those prior works [16,17] fracture was caused by the formation of “surface shock waves” accompanied by a sharp increase of the stress at the surface; the measurements could only provide a lower bound estimate of the peak stress value. In a recent study [18], we proposed an alternative approach, based on focusing SAWs. The short SAW propagation distance (100 μm) prevents shock front formation, and the high stress that occurs where the SAWs are focused is essentially achieved in the linear elastic regime. These measurements are very different from traditional shock spallation studies in that the tensile phase of the SAW pulse lasts only a few nanoseconds and is not preceded by a significant pre-compression. In experiments on gold-coated glass, we observed failure of the gold coating and, at higher laser energies, of the glass substrate. However, the early failure of the gold layer prevented measurements of the SAW pulse profile at high amplitudes and complicated the interpretation of the observations of the glass damage. In the current work, we report experiments in a modified arrangement, wherein a gold coating is still used to generate SAWs but their focusing occurs on a bare glass substrate. Above a certain SAW amplitude threshold, glass failure at the focal point and the formation of a crater due to the ejection of

the fractured material are observed. Numerical calculations matching experimentally measured displacement profiles in the focused SAW allow us to characterize the dynamics of the stress distribution in the sample.

The experimental setup, shown schematically in Fig. 1, follows the design developed by Veyssset et al. [18]. A laser excitation pulse, derived from a Ti:sapphire amplifier, with a 300-ps duration, 800-nm wavelength and adjustable energy (from 0.15 mJ to 1.50 mJ), was focused onto the surface of a 300 μm -thick borosilicate glass substrate (D263 Schott) to ablate a 160 nm-thick metallic ring. The metallic ring, henceforth referred to as the gold ring, consisted of 10-nm chromium, in contact with the glass, and 150-nm gold. The gold ring had an inner diameter of 160 μm and an outer diameter of 240 μm (see supplementary material for sample fabrication). The laser focus was shaped as a 200 μm -diameter, 5 μm -wide ring using a 0.5° conical prism (axicon) and a 3 cm focal-length lens, as described by Pezeril et al. [19] and Veyssset et al. [20,21]. Multiple rings were fabricated on the same substrate and the sample was translated to move the laser focus to a new ring for each laser shot, with the laser focus and ring overlapping as in Fig. 1b each time. Imaging of the sample surface was achieved using a variably-delayed, 150-fs duration probe pulse reflected from the surface of the sample. The probe pulse, derived from the same amplifier system, was frequency-doubled to 400-nm wavelength. Interference fringes of equal thickness obtained using a Michelson interferometer configuration were recorded by a CCD camera.

For each laser shot, stress waves were produced following ablation—therefore destruction—of the metallic film and a single image was recorded with a set time delay between the excitation and the probe pulses. Because of the ring shape of the excitation, focusing and diverging surface waves were generated and propagated on the surface of the bare glass (see Fig. 1b and c). Bulk waves were also generated but were not imaged in the present configuration. As the surface was displaced under SAW propagation, the phase of the reflected pulse shifted (the phase shift is denoted as $\Delta\varphi$) causing fringes to shift on the CCD image (see Fig. 1c). By measuring the fringe shift, we could determine the corresponding out of plane surface displacement $u_z(r)$ through the relationship $u_z = \lambda\Delta\varphi/4\pi$, where $\lambda = 400 \text{ nm}$ is the probe pulse wavelength. After each shot, the sample was positioned to a new ring and different time delay and laser energy could be set.

We recorded images such as that shown in Fig. 1c for multiple time delays and laser energies and extracted the surface displacements along a ring diameter. More details regarding the image analysis can be found in Veyssset et al. [18]. Fig. 2a presents surface displacement profiles showing the propagation of the focusing SAW for 7 delays at a laser energy of 0.25 mJ, corresponding to a laser fluence of 4.5 J/cm². The SAW focused around 30 ns after being generated and subsequently diverged. Fig. 2b shows the surface displacements obtained for a laser energy of 0.75 mJ. Around this laser energy, the image quality was degraded at longer times and the surface displacements closer to the focus or right after the focus could not be accurately extracted. Fig. 2c shows the peak-to-peak amplitude of the SAW taken at a delay of 12.7 ns for varying laser energies and shows that the SAW amplitude started to saturate at laser energies above 1 mJ.

In our previous work, with the same experimental design but with the sample surface uniformly coated with a gold film, the large amplitude of the SAW at the focal point caused delamination and damage of the film at low laser energy ($\sim 0.1 \text{ mJ}$) and glass substrate fracture at high laser energy ($\sim 2 \text{ mJ}$) [18]. The film damage obscured the imaging of the SAW at higher laser energies making it impossible to evaluate the absolute surface displacements leading to glass fracture. Here, with no metal film inside the ring, we observe surface displacements even at high laser energies and, after sample examination under laser-scanning confocal microscope and atomic force microscope, can confirm visible glass fracture at laser energies above 0.75 mJ. The substrate visibly fractured at the center in about 10% of the cases for a laser energy of 1.00 mJ and in 100% of the cases for a laser energy of 1.50 mJ (see Fig. 2c,

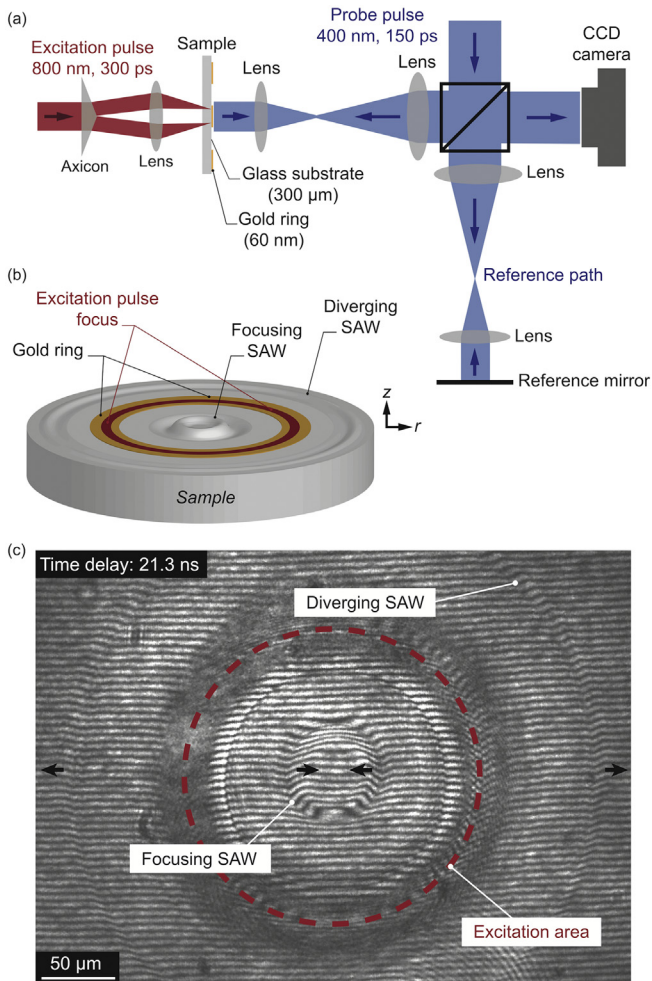


Fig. 1. (a) Experimental setup. The excitation beam is shaped as a ring with an axicon/lens combination. Interferometric imaging is achieved using a Michelson interferometer. (b) Schematic of the sample configuration. The excitation pulse is focused on the gold ring, generating focusing and diverging surface acoustic waves. (c) Interferometric image showing surface displacement caused by focusing and diverging SAWs. This image was taken for a laser energy of 0.25 mJ with a delay of 21.3 ns between the excitation and the probe pulses. The dashed ring indicates the laser excitation area. Circular fringes appearing at the bottom of the image comes from a defect on one of the imaging optics. See supplementary material for images taken before laser excitation and post mortem.

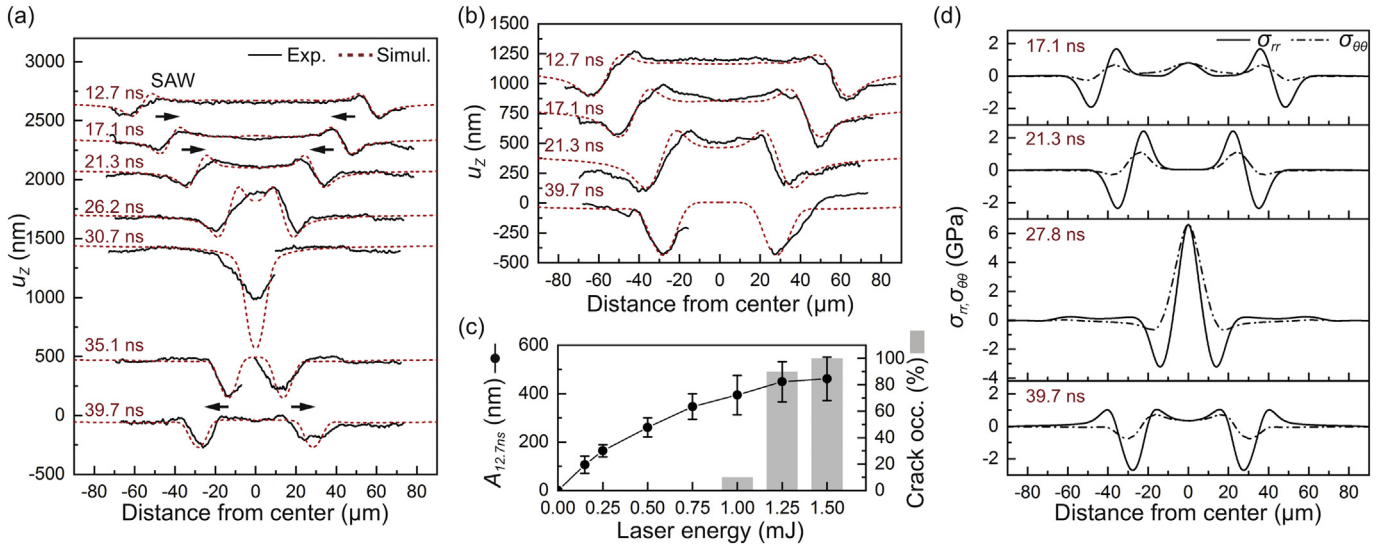


Fig. 2. (a–b) Experimental and simulated surface displacements, u_z , as a function of time delay for two laser energies: (a) 0.25 mJ and (b) 0.75 mJ. (c) (left axis) SAW peak-to-peak amplitude experimentally measured after a delay of 12.7 ns with varying laser energy. The data points represent the average between the left and right lobes of the SAW and taking into account different shots. The error bars represent the standard deviation on the peak-to-peak amplitude. (right axis) Visible occurrence, in % of observed cases, of glass fracture as a function of laser energy. (d) Simulated non-zero stresses σ_{rr} and $\sigma_{\theta\theta}$ at the sample surface ($z = 0$) corresponding to the last three simulated surface displacements shown in (b) and for the delay corresponding to the maximum tensile stress at the center (27.8 ns).

right axis). When visible damage was observed, a laser-scanning confocal microscope revealed a crater of about 10–20 μm in diameter and about 4–5 μm in depth, as shown for example in Fig. 3. In rare instances, the ejected piece of glass was found near the central pit (see Fig. 3b and the corresponding elevation profile in Fig. 3c). It is interesting to note that the removed piece is a single piece of glass. For all studied energies, we observed no damage between the laser excitation area and the central crater.

In order to estimate the stress levels that were reached through SAW focusing, we implemented a 2D axisymmetric finite element model (see supplementary material for more details on the model) and simulated the linear SAW propagation following a Gaussian distribution impulse at the laser focus position. The amplitude and the width of the initial pressure distribution were calibrated to match the experimentally-measured peak-to-peak amplitudes of the SAW for laser energies of 0.25 and 0.75 mJ. The simulated surface displacements and stresses σ_{rr} and $\sigma_{\theta\theta}$ at the surface are shown in Fig. 2a, b and d. The reasonable agreement between the experiments and the simulations confirms the linear propagation of the SAW. The good agreement after the focus is consistent with the absence of the visible damage.

As shown in Fig. 4a, at the focal point and at the surface of the sample ($r = 0$, $z = 0$), after the passage of the longitudinal surface skimming

wave (SSWL), the material experienced a high level of tension, then a high level of compression, and finally a lower level of tension brought by the SAW. Fig. 4b and c show the principal stress profiles, σ_{rr} and σ_{zz} , at the center of focus, as a function of depth (with $z = 0$ being the surface of the substrate) for three delays 27.8, 31.7, and 35.1 ns, corresponding to the three stress extrema of the SAW. We assume that damage is initiated by the initial tensile phase of the SAW pulse at the sample surface, where the radial tensile stress is the highest. We note that during this initial tensile phase the surface velocity at the focal point is directed outwards, which can explain the ejection of the fractured material.

Despite a simulated equibiaxial tension as high as 6.6 GPa at the center of focus at the surface (Fig. 4b, depth $z = 0$) at a laser energy of 0.75 mJ, we observed no sign of failure of the substrate at this laser energy. It is well known that in a variety of materials the high strain rate strength can exceed the static strength by orders of magnitude [15,22–24] and the present value is higher than what has been previously reported in the literature for the dynamic fracture of glass. The high stress value can be justified by a combination of factors pertaining to the experimental method. First, the glass experienced an ultra-high strain rate, up to 10^8 s^{-1} , upon the passage of the nanosecond-duration SAW, which is shorter than the typical microsecond time

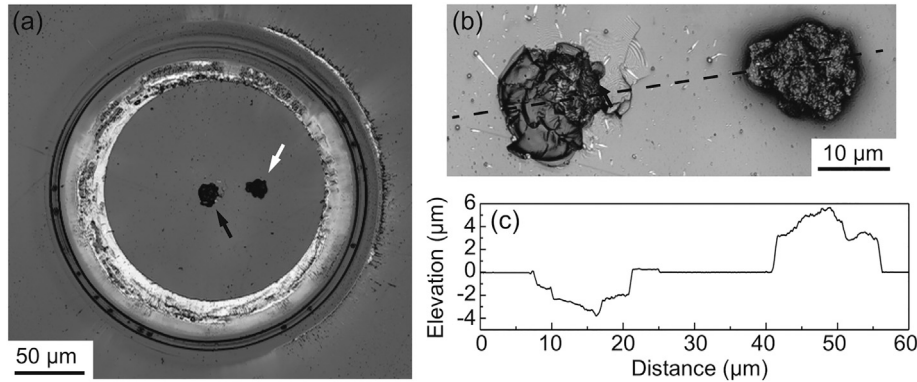


Fig. 3. Laser-scanning confocal microscope images of typical glass damage for a laser energy of 1.00 mJ. (a) Large view showing excitation location, parts of remaining gold film, and central crack. The black arrow points to the central crack and the white arrow to the removed piece. (b) Zoomed-in image of the central damage and corresponding delaminated piece. (c) Elevation profile along the dashed line shown in (b).

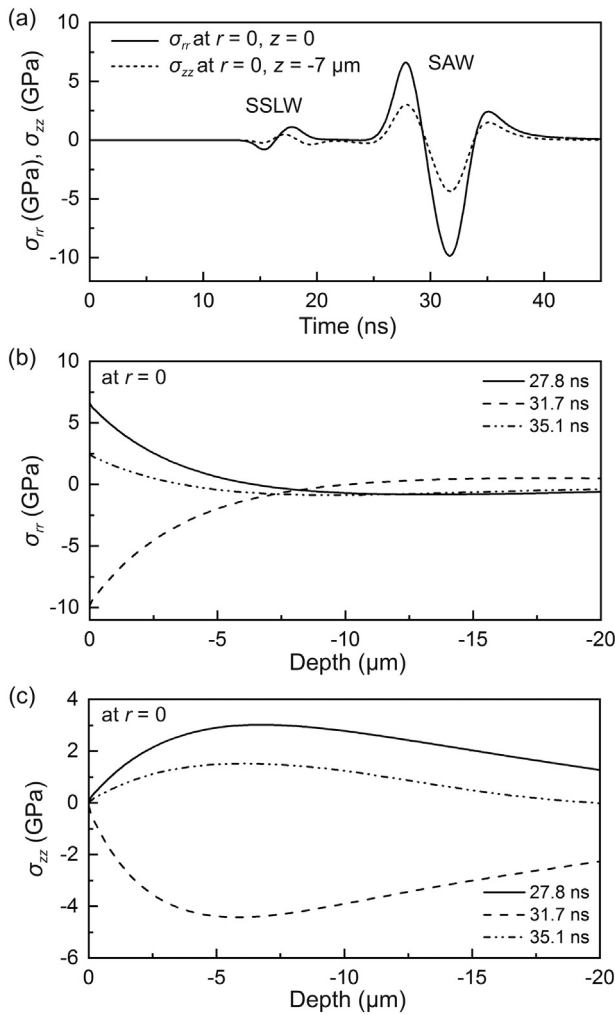


Fig. 4. (a) Non-zero principal stresses σ_{rr} (solid line) computed at the center of focus ($r=0$) and at the surface ($z=0$) and σ_{zz} (dotted line) at the center of focus ($r=0$) and below surface ($z=7\text{ }\mu\text{m}$, corresponding to the depth of maximum value) as a function of time. (b–c) Principal stresses, σ_{rr} , and σ_{zz} , at $r=0$ for three delays, corresponding to stress extrema, as a function of depth for a laser energy of 0.75 mJ.

scale of spallation experiments. Second, in the present experiments, the initial tensile phase is not preceded by a compression (except of the much weaker SSLW), whereas in spallation experiments the pre-compression by an intense shock wave influences the spall strength [25,26]. Third, with the very small volume of material being loaded in the present experiments, there is a reduced possibility of surface defects being present, permitting a tensile strength approaching the theoretical limit [5]. Finally, as with more conventional methods, we cannot rule out the possibility that some degree of fracture has occurred at the nanoscale in any of our experiments, but leaves no visible trace with our methods of observation.

In summary, high stresses were locally attained using focusing laser-generated SAWs, and stress histories were determined from a combination of interferometric measurements and axisymmetric finite element simulations. We found that under nanosecond tensile loadings up to ~6 GPa with no pre-compression, no visible damage or fracture was observed on samples of glass. At higher excitation laser energies, we observed damage at the focal point in the form of a crater left by the

fracture and ejection of a piece of material. The present method is applicable for a wide range of materials and opens prospects for ultra-high strain rate dynamic failure testing of novel materials with limited available volumes and for refining fracture models.

See supplementary material for sample fabrication, before-excitation and post-mortem images, laser-induced damage, simulation details, effects of non-linearity, temporal and spatial evolutions of the stress at the center of focus, and laser asymmetry considerations.

Acknowledgments

D.V. thanks Panagiotis Natsiavas for initial modeling efforts. This material is based upon work supported in part by the U. S. Army Research Office through the Institute for Soldier Nanotechnologies, under Cooperative Agreement Numbers W911NF-13-D-001 and W911NF-18-2-0048 and by the Office of Naval Research, Grant No. N000141512694. The authors acknowledge financial support from CNRS (Centre National de la Recherche Scientifique) under grant Projet International de Coopération Scientifique. C.A.S., K.A.N. and M.H.-G. acknowledge support from the U.S. Department of Energy, Office of Science, Office of Basic Energy Sciences, Division of Materials Sciences and Engineering under Award DE-SC0018091. X. Z and X. Z. acknowledge support by the National Science Foundation (grant number ECCS-1309835).

Appendix A. Supplementary data

Supplementary data to this article can be found online at <https://doi.org/10.1016/j.scriptamat.2018.08.026>.

References

- [1] E. Christiansen, J. Hyde, R. Bernhard, *Adv. Sp. Res.* 34 (2004) 1097–1103.
- [2] L. Wondraczek, J.C. Mauro, J. Eckert, U. Kühn, J. Horbach, J. Deubener, T. Rouxel, *Adv. Mater.* 23 (2011) 4578–4586.
- [3] S.M. Wiederhorn, *J. Am. Ceram. Soc.* 52 (1969) 99–105.
- [4] Schott Technical Glasses, Physical and Technical Properties, www.us.schott.com.
- [5] G. Brambilla, D.N. Payne, *Nano Lett.* 9 (2009) 831–835.
- [6] J.E. Field, S.M. Walley, W.G. Proud, H.T. Goldrein, C.R. Siviour, *Int. J. Impact Eng.* 30 (2004) 725–775.
- [7] Z. Rosenberg, D. Yaziv, S. Bless, *J. Appl. Phys.* 58 (1985) 3249–3251.
- [8] Z. Rosenberg, Y. Ashuach, E. Dekel, *Int. J. Impact Eng.* 35 (2008) 820–828.
- [9] H.D. Espinosa, Y. Xu, N.S. Brar, *J. Am. Ceram. Soc.* 80 (2005) 2061–2073.
- [10] G.I. Kanel, S.V. Razorenov, V.E. Fortov, *Shock-Wave Phenomena and the Properties of Condensed Matter*, 2004.
- [11] M.J. Davis, *Int. J. Appl. Glas. Sci.* 7 (2016) 364–373.
- [12] G.F. Raiser, J.L. Wise, R.J. Clifton, D.E. Grady, D.E. Cox, *J. Appl. Phys.* 75 (1994) 3862–3869.
- [13] S.V. Rasorenov, G.I. Kanel, V.E. Fortov, M.M. Abashev, *High Pressure Res.* 6 (1991) 225–232.
- [14] N.K. Boume, J.C.F. Millett, J.E. Field, *Proc. R. Soc. Lond. A Math. Phys. Sci.* 455 (1999) 1275–1282.
- [15] E. Moshe, S. Eliezer, E. Dekel, A. Ludmirsky, Z. Henis, M. Werdiger, I.B. Goldberg, N. Eliaz, D. Eliezer, *J. Appl. Phys.* 83 (1998) 4004–4011.
- [16] A.M. Lomonosov, P. Hess, *Phys. Rev. Lett.* 89 (2002), 095501.
- [17] G. Lehmann, A.M. Lomonosov, P. Hess, P. Gumbsch, *J. Appl. Phys.* 94 (2003) 2907.
- [18] D. Veyssset, A.A. Maznev, I.A. Veres, T. Pezeril, S.E. Kooi, A.M. Lomonosov, K.A. Nelson, *Appl. Phys. Lett.* 111 (2017), 031901.
- [19] T. Pezeril, G. Saini, D. Veyssset, S. Kooi, P. Fidkowski, R. Radovitzky, K.A. Nelson, *Phys. Rev. Lett.* 106 (2011) 214503.
- [20] D. Veyssset, T. Pezeril, S. Kooi, A. Bulou, K.A. Nelson, *Appl. Phys. Lett.* 106 (2015) 161902.
- [21] D. Veyssset, U. Gutiérrez-Hernández, L. Dresselhaus-Cooper, F. De Colle, S. Kooi, K.A. Nelson, P.A. Quinto-Su, T. Pezeril, *Phys. Rev. E* 97 (2018), 053112.
- [22] E. Moshe, S. Eliezer, Z. Henis, M. Werdiger, E. Dekel, Y. Horovitz, S. Maman, I.B. Goldberg, D. Eliezer, *Appl. Phys. Lett.* 76 (2000) 1555.
- [23] C. Huang, G. Subhash, *J. Mech. Phys. Solids* 51 (2003) 1089–1105.
- [24] W. Chen, G. Ravichandran, *J. Mech. Phys. Solids* 45 (1997) 1303–1328.
- [25] J. Cagnoux, F. Longy, *J. Phys. Colloq.* 49 (1988) C3-3-C3-10.
- [26] R.L. Whelchel, T.H. Sanders, N.N. Thadhani, *Scr. Mater.* 92 (2014) 59–62.